Reprinted from JOURNAL OF APPLIED PHYSICS, Vol. 41, No. 13, 5309–5314, December 1970

Shock Compression of Shoal Granite

ROBERT S. DENNEN*
Physics Department, University of Illinois† at Chicago Circle, Chicago, Illinois 60680
(Received 14 November 1969; in final form 12 June 1970)

Experiments utilizing explosives with and without flyer plates have been used to determine the shock compression properties of shoal granite. High-speed framing camera records were used to determine the free surface angles which occur in wedge-cut samples upon the emergence of the resulting shock waves. The shock equations are given for the oblique geometry. Previously observed yield point data are used to obtain the Hugoniot of shoal granite in the range between 0 and 400 kbars.

I. INTRODUCTION

A number of reports and publications have given high-pressure data for granite.[1–4] Attempts to plot these data on a single curve sometimes show considerable scatter.[2,5] Such scatter is no doubt due in part to experimental errors and sample to sample variation but may also be partially attributable to differences in the materials studied. Materials with a fairly wide variation in the proportion of mineral abundancies fall under the general classification of granite.

In this paper the results of high-pressure shock compression experiments on shoal granite are given.[6] The mineral content of this material was reported in a previous paper[7] where the results of experiments for shock pressures up to about 40 kbars were given. In the earlier work a shock tube method was used; here high explosives were used to obtain pressures up to about 400 kbars. The object of this work is to furnish shock data for one particular type of granite throughout the complete range up to 400 kbars.

II. EXPERIMENTAL METHOD

Two different configurations were used to generate a shock wave in a wedge-cut sample of granite. In the first, as shown schematically in Fig. 1, an explosive train consisting of a detonator, plane wave generator, and pad of high explosive were used to impact a flyer plate upon the sample. In the second, the explosive train was placed in direct contact with the sample. In both configurations, a shock wave was generated in the sample which caused free surface motion of the back face of the sample. A framing record of the slit and fiducial markings between the sample and knife edge were recorded on a Beckman Whitley model 189 framing camera. The slit area was back lighted by an argon light bomb detonated prior to the free surface motion. The

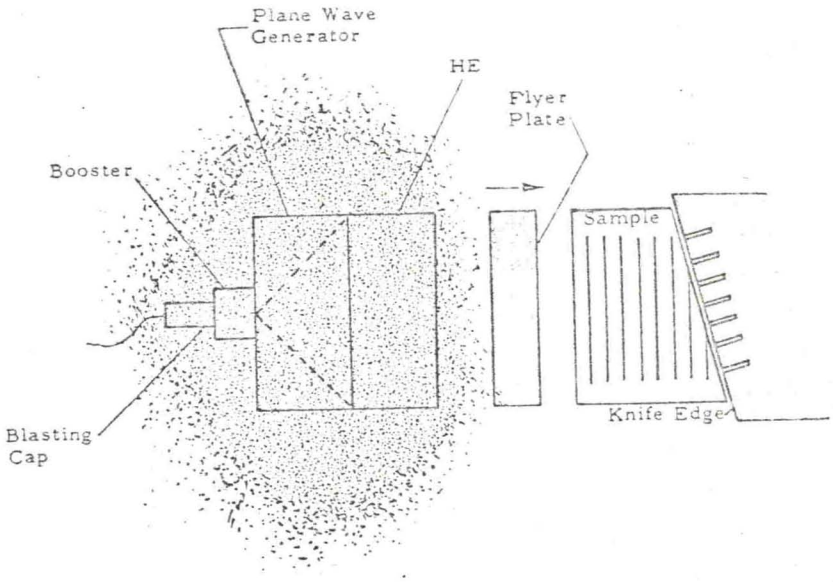

FIG. 1. Configuration for explosively driven flyer plate experiments on wedge-cut samples.

timing sequence was determined by the position of the rotating mirror in the framing camera. Thus, at a predetermined rotor position after detonation of the explosive train, the argon flash was detonated. A gating scheme was used to ensure that the triggering signal generated during each revolution of the camera rotor did not ignite the argon flash until after the explosive train was detonated. The explosive train was detonated when the rotating mirror reached the desired rotational velocity.

A record of the free surface configuration is shown in Fig. 2. From a series of such consecutive records, the shock wave and free surface velocities were calculated.

III. SHOCK WAVE EQUATIONS

In a number of investigations the shock equations have been used. These equations relate the one-dimensional strain and the diagonal stress tensor component in the shock propagation direction to the measurable variables, the shock and material velocities. For a single shock wave propagating into initially unstressed material the stress and strain are

$$\sigma = \rho_0 U_s U_p \tag{1}$$

and

$$\epsilon = \Delta V/V_0 = U_p/U_s, \tag{2}$$

where U_s and U_p are the shock wave and material velocities and ρ_0 and V_0 are the initial density and volume, respectively. The stress σ differs from the hydrostatic stress when the shear modulus has a finite value. For very high stresses the shear modulus vanishes and the diagonal stresses are equal to the pressure. In most of the experiments discussed here the stress level is not high enough to neglect the shear forces so that the value of σ found from Eq. (1) cannot be thought of as the hydrostatic pressure, and shear waves can be expected.

FIG. 2. Sample record of slit area showing intersections of the elastic and plastic waves with the free surface of a granite wedge.

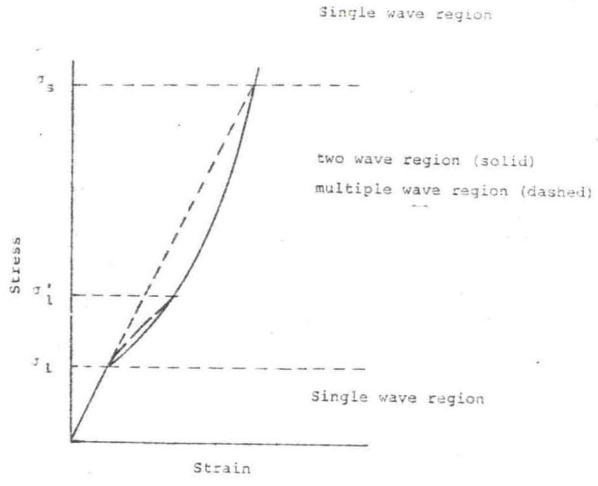

FIG. 3. Schematic diagram of possible response curves for shock compression.

In Ref. 8 conditions were discussed in which more than one shock wave are generated. Two shock waves are expected to be generated in a material which is shock compressed to a stress slightly above its dynamic elastic limit or phase transition pressure. In such cases the stress and strain behind the second wave are

$$\sigma_2=[\rho_0 U_{s1}(U_{s2}-U_{p1})(U_{p2}-U_{p1})/(U_{s1}-U_{p1})]+\sigma_1, \tag{3}$$

and

$$\epsilon_2=1-[(U_{s1}-U_{p1})(U_{s2}-U_{p2})/U_{s1}(U_{s2}-U_{p1})], \tag{4}$$

where U_{s1} and U_{s2} are the velocities in laboratory coordinates of the first and second shock waves, and U_{p1} and U_{p2} are the material velocities behind the first and second waves. The regions in which these equations are applicable are shown in the Hugoniot diagram of Fig. 3. The Hugoniot shown in Fig. 3 corresponds to a material with a yield point or phase transition at σ_1. If the transition or yielding does not occur at a well specified stress but occurs over a range of stresses (σ_1 to σ_1' in Fig. 3) a shock wave fan will be generated for stresses between σ_1 and σ_s. For this case Eqs. (3) and (4) may be generalized to n shock waves. Thus,

$$\sigma_n=\sigma_{n-1}+[\rho_0(U_{sn}-U_{p,n-1})(U_{pn}-U_{p,n-1})/(1-\epsilon_{n-1})] \tag{5}$$

and

$$\epsilon_n=1-\prod_{i=1}^{i=n}[(U_{si}-U_{p1})/(U_{si}-U_{p,i-1})]. \tag{6}$$

For the wedge configuration used in this series of experiments, it is possible to determine the general features of the Hugoniot by analysis of the shape of the free surface. Thus in Fig. 2, it is seen that the free surface has two points of slope change which correspond to the intersection of two waves with the free surface. The analysis of these data are based on the two wave configuration shown in Fig. 4. For such a two-wave system, the first wave is the elastic wave and transmits a stress corresponding to the dynamic elastic limit or yield point. Upon its reflection at the free surface, two waves reflect into the sample, a dilatational and a shear wave. Because the second wave or plastic wave is well above the yield point, shear forces are not considered so that only a single longitudinal decompression wave is considered

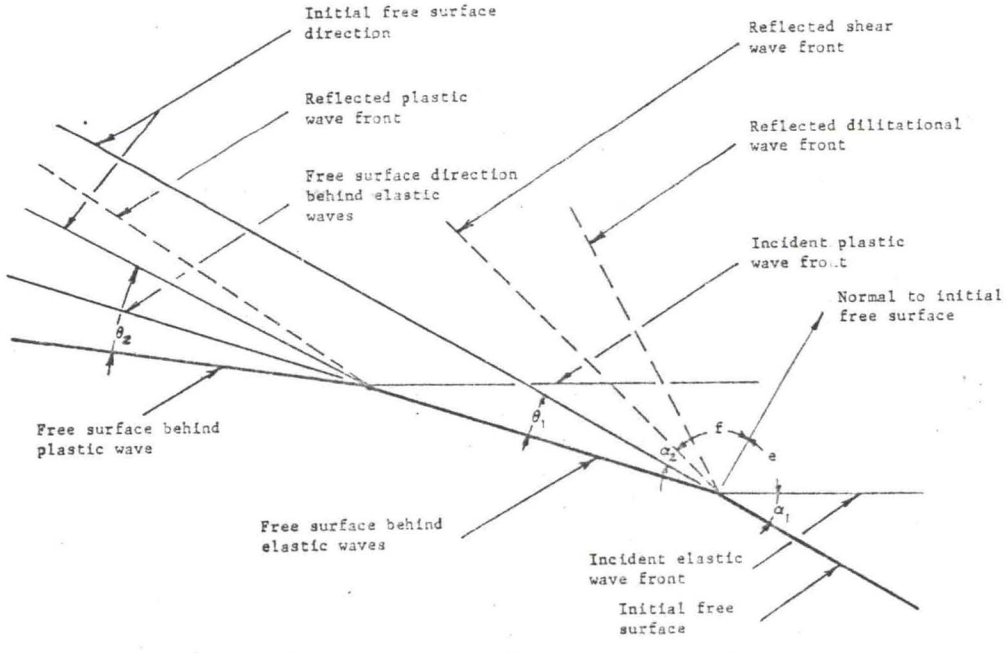

FIG. 4. Free surface and shock wave configuration.

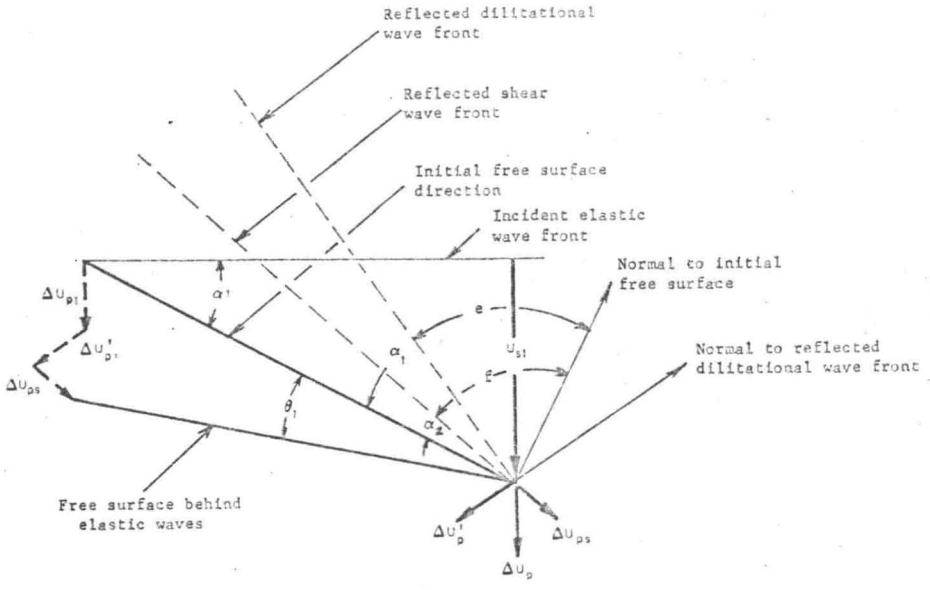

FIG. 5. Vector diagram for elastic wave interaction with the free surface.

to be reflected at the free surface. The vector diagrams in Figs. 5 and 6 show the material velocities associated with each of these waves and their relation to the free surface angles which may be measured in each experiment. In addition, in order to use Eqs. (3) and (4) to find the stress and strain behind each wave, it is necessary to determine the material velocities, U_{p1} and U_{p2}, which occur behind the first and second waves within the sample.

From Fig. 5, the free surface angle θ_1, is

$$\tan\theta_1 = \frac{(1+r_1)\cos\alpha_1 + r_2\sin\alpha_2}{1/\epsilon_1 - (1-r_1)\sin\alpha_1 - r_2\cos\alpha_2}, \qquad (7)$$

where

$$r_1 = \Delta U_{p1}'/\Delta U_{p1}$$

and

$$r_2 = \Delta U_{ps}/\Delta U_{p1}$$

are the reflected material velocity ratios for the dilatational and shear waves, respectively; α_1 and α_2 are the shock front angles between the free surface and the dilatational and shear wave fronts, respectively; ϵ_1 is the strain at the yield point as defined in Eq. (2); ΔU_{p1} is the material velocity occurring behind the incident elastic wave; and $\Delta U_{p1}'$ and ΔU_{ps} are the material velocities which occur behind the reflected dilatational and shear waves, respectively, as shown in Fig. 5.

The velocity ratios are related to the angles of obliquity e and f as shown in Fig. 5 by the relationships[9-11]

$$\frac{\Delta U_{p1}'}{\Delta U_{p1}} = \frac{4\tan f\tan e - (\tan^2 f - 1)g(\nu)}{4\tan f\tan e + (\tan^2 f - 1)g(\nu)} \qquad (8)$$

and

$$\frac{\Delta U_{ps}}{\Delta U_{p1}} = \frac{-4\tan e\, g(\nu)}{4\tan e\tan f + (\tan^2 f - 1)g(\nu)}, \qquad (9)$$

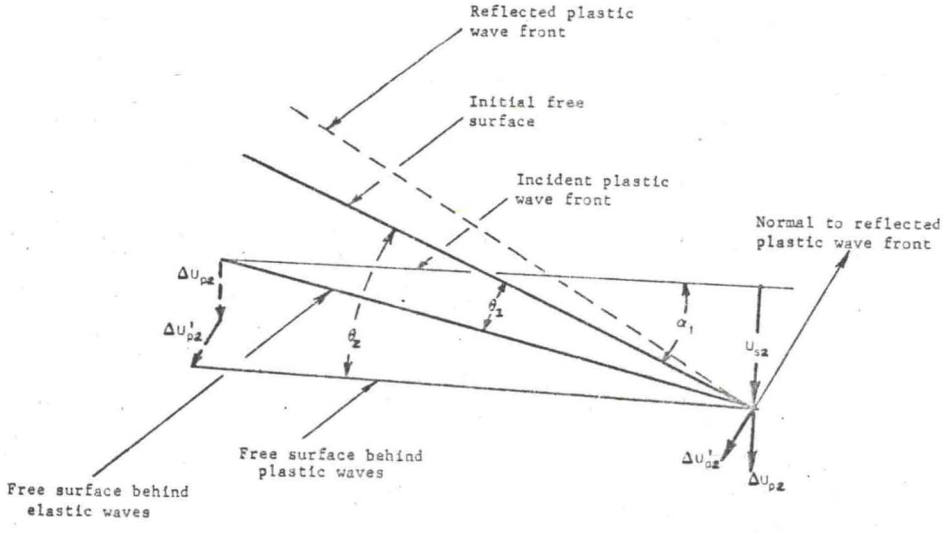

FIG. 6. Vector diagram for plastic wave interaction with the free surface.

TABLE I. Shock data for Shoal granite.

Exp. no.	Free surface angles (radians) [Eq. (7)]ᵃ θ_1	Free surface angles (radians) (obs.) θ_2	Wedge angle (degrees) (meas.) α_1	Plastic wave velocities[a] (mm/μsec) (obs.) U_{s2}	Plastic wave velocities[a] (mm/μsec) [Eq. (15)] U_{p2}	Stress[a] (kbars) [Eq. (3)] P_2	Strain[a] [Eq. (4)] ϵ_2
35	0.0199	0.1304	15.00	5.182	1.481	205.6	0.281
38	0.0199	0.1644	15.00	5.791	2.047	313.2	0.352
40	0.0199	0.1672	15.00	5.425	1.965	283.3	0.359
42	0.0199	0.0964	15.00	3.932	0.898	103.8	0.210
43	0.0199	0.1155	15.00	4.481	1.171	145.6	0.250
44	0.0194	0.1200	14.50	4.663	1.291	164.9	0.268
46	0.0219	0.1497	17.00	5.822	1.672	257.0	0.286
47	0.0199	0.1054	15.00	3.993	0.985	113.9	0.230
49	0.0199	0.1819	15.00	6.126	2.380	384.1	0.389
50	0.0209	0.1065	16.00	6.035	1.296	205.1	0.215
51	0.0194	0.1225	14.50	5.334	1.471	209.5	0.272
52	0.0199	0.1006	15.00	3.566	0.870	94.7	0.221
53	0.0165	0.1112	12.00	4.968	1.500	200.9	0.295
56	0.0165	0.0887	12.00	4.572	1.128	142.8	0.236
60	0.0183	0.1171	13.50	5.029	1.431	193.9	0.278
61	0.0188	0.0902	14.00	4.054	0.916	107.8	0.209
66	0.0194	0.1112	14.50	4.663	1.195	152.4	0.248

[a] Elastic wave data taken from Ref. 7; shock velocity (U_{p1}) = 5.98 mm/μsec, strain ϵ_1 = 0.040, material velocity (U_{p1}) = 0.239 mm/μsec, yield pt. (P_1) = 38 kbars, and the initial density (ρ_0) = 2.65 g/cc.

where

$$g(\nu)=[(\lambda/\mu+2)\tan^2 e+\lambda/\mu], \quad (10)$$

λ and μ are the Lamé constants, and ν is Poisson's ratio, so that $\lambda/\mu=2\nu/(1-2\nu)$. The notation in Eqs. (8) and (9) is used to correspond to that of Refs. 10 and 11, and the angles e and f are related to the shock front angles α_1 and α_2 by the equations

$$\alpha_1=\pi/2-e$$

and

$$\alpha_2=\pi/2-f, \quad (11)$$

where

$$\tan^2 f=[2(1-\nu)/(1-2\nu)](\tan^2 e+1)-1. \quad (12)$$

From Fig. 6, one can also relate the free surface angle θ_2 to the material velocity ΔU_{p2} behind the plastic wave. Thus

$$\Delta U_{p2}=U_{s2}\tan(\theta_2-\theta_1)/\sin 2(\alpha_1-\theta_1). \quad (13)$$

IV. RESULTS

By use of Eqs. (7)–(13), the measured values of θ_1, θ_2, α_1, U_{s1}, and U_{s2}, and a value of Poisson's ratio ν for granite,[12] values of U_{p1} and U_{p2} might be calculated since

$$U_{p1}=\epsilon_1 U_{s1}=\Delta U_{p1} \quad (14)$$

and

$$U_{p2}=\Delta U_{p1}+\Delta U_{p2}. \quad (15)$$

A somewhat different procedure was used however because θ_1 was small, of the order of 1 deg, so that U_{s1} was difficult to measure. Instead, values of the yield point data were taken from Ref. 7 and used to calculate θ_1 from Eqs. (7)–(12). Equation (13), with observed values of θ_2 and U_{s2} was then used to calculate U_{p2}. The stress and strain were then calculated from Eqs. (3) and (4). The results are shown in Table I. In Fig. 7, the Hugoniot for this material is shown. Results from the earlier low-pressure study[7] and higher-pressure data for shoal granite from Ref. 2 are also shown.

V. SUMMARY

The solid line in Fig. 5 represents what is considered to be the best estimate for the Hugoniot for shoal granite.[13] The scatter of the data about that line is partially attributable to the relatively large grain sizes of the mineral constituents of this material. The technique used here has one relative advantage over other methods, such as interferometric, which utilize information from very small elements of the free surface of a sample. Here the characteristic dimension of the portion of the sample, which contributes to the observed angles, is large compared to the grain size. One disadvantage of the present method is that the interaction of the reflected and incident wave fronts within the sample is neglected. That neglect is analogous to simplifying assumptions made in experimental configurations utilizing normal wave interactions as already pointed out.[14] The accuracy of the present method is determined to a large extent by the errors in measuring shock velocities and free surface angles. These are estimated as 2% and 0.15 degrees, respectively, and from Eqs. (5),

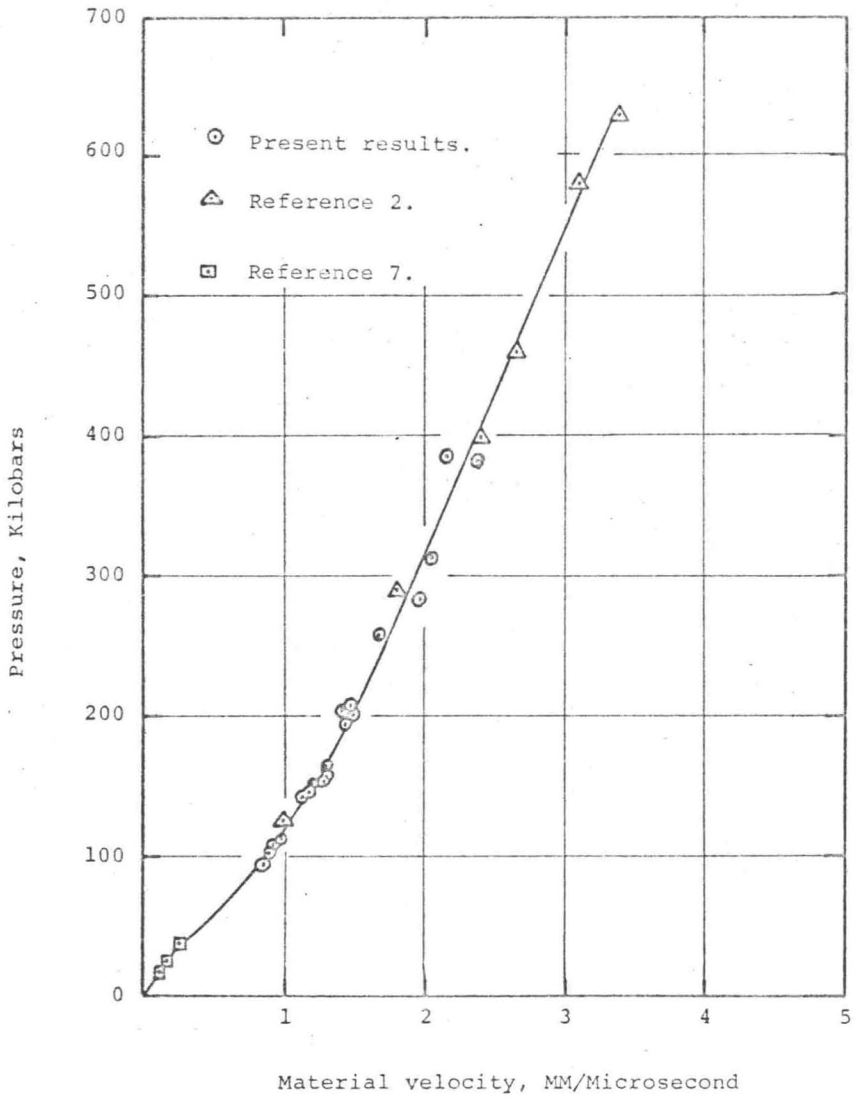

FIG. 7. Shock data for shoal granite.

(13), and (15), lead to errors in pressures and material velocities of less than 4% and 2.5%, respectively.

ACKNOWLEDGMENT

The original data were obtained under Atomic Energy Commission contract. The author is grateful for that support.

* Presently at Martin Marietta Corporation, P.O. Box 179, Denver, Colo. 80201.
† Experimental work was done at IIT Research Institute.

[1] F. H. Shipman, W. M. Isbell, and A. H. Jones, Defense Atomic Support Agency Report, DASA 2214, 1969.
[2] R. C. Bass, H. L. Hawk, and A. J. Chabai, Sandia Corp. SC-4903 (RR), 1963.
[3] D. R. Grine, Shock and Vibration Symp. 29th Oakland, Calif., 1960.
[4] D. S. Hughes and R. G. McQueen, Trans. Amer. Geophys. Union 39, 959 (1958).
[5] D. B. Lombard, U. Calif. Lawrence Radiation Laboratory Rep. No. UCRL-6311, 1961.
[6] Shock experiments on shoal granite were also carried out by Sandia (Ref. 2); the results are complementary.
[7] R. S. Dennen, J. Appl. Phys. 40, 3326 (1969).
[8] M. H. Rice, R. G. McQueen, and J. M. Walsh, Solid State Phys. 6, 1 (1958).
[9] H. Kolsky, *Stress Waves in Solids* (Dover, New York, 1952), p. 24.
[10] W. M. Ewing, W. S. Jardetzky, and F. Press, *Elastic Waves in Layered Media* (McGraw-Hill, New York, 1957), p. 24.
[11] V. G. Gregson, Jr., J. Appl. Phys. 38, 1798 (1967).
[12] F. Birch and D. Bancroft, J. Geol. 48, 752 (1940).
[13] This curve is slightly modified from that used for the Hugoniot synthesis work in Ref. 14.
[14] R. S. Dennen, Defense Atomic Support Agency Report, DASA 1652, 1965.